



LETTER • OPEN ACCESS

Observed evolution of global climate change hotspots

To cite this article: Zhuoya Du et al 2025 Environ. Res. Lett. 20 074031

View the article online for updates and enhancements.

You may also like

- <u>Dust source activation frequency across East Asia</u>
 Lingle Chen, Kerstin Schepanski, Anya J Crocker et al.
- Provincial economic and air quality-related health impacts of China's potential partitioned carbon regulation Hantang Peng, Mingwei Li, Da Zhang et
- Not just a climate problem: the safety and health risks of methane super-emitter events
 Sofia Bisogno, Chowdhury G Moniruzzaman, Nick Heath et al.



ENVIRONMENTAL RESEARCH

LETTERS



OPEN ACCESS

RECEIVED

28 January 2025

REVISED

6 April 2025

ACCEPTED FOR PUBLICATION 30 May 2025

PUBLISHED

10 June 2025

Original content from this work may be used under the terms of the Creative Commons Attribution 4.0 licence.

Any further distribution of this work must maintain attribution to the author(s) and the title of the work, journal citation and DOI.



LETTER

Observed evolution of global climate change hotspots

Zhuoya Du¹, Xuchou Han¹, Fei Ji¹,²,*, Pei Ji¹,²,*, Zhenhao Xu³,⁴, Xiaodan Guan¹,², and Jianping Huang², Landing Huang², and Jianping Huang², Landing Huang², L

- ¹ College of Atmospheric Sciences, Lanzhou University, Lanzhou, People's Republic of China
- Collaborative Innovation Center for Western Ecological Safety, Lanzhou University, Lanzhou, People's Republic of China
- State Key Laboratory of Numerical Modeling for Atmospheric Sciences and Geophysical Fluid Dynamics, Institute of Atmospheric Physics, Chinese Academy of Sciences, Beijing, People's Republic of China
- ⁴ University of Chinese Academy of Sciences, Beijing, People's Republic of China
- * Author to whom any correspondence should be addressed.

E-mail: jif@lzu.edu.cn

Keywords: climate change, hotspots, EEMD, evolution, extreme events

Supplementary material for this article is available online

Abstract

This study introduces a novel dynamical climate change hotspot index standard Euclidean distance, capturing variations in temperature and precipitation through average, variability, and extreme values, and utilizes ensemble empirical mode decomposition to analyze nonlinear long-term trends globally. Results highlight pronounced regional disparities, with regions like the Tibetan Plateau, Mongolia, and the Arabian Peninsula emerging as persistent hotspots due to rapid warming responses. In contrast, the southeastern United States exhibits early-stage declines, though vulnerability to extreme weather is growing. A latitude-time analysis reveals asymmetric hemispheric trajectories, driven by distinct climate dynamics and anthropogenic influences. The transition from systemic temperature-influenced hotspots to localized, extreme event-influenced phenomena underscores the intensifying impact of extreme climate events. These findings provide critical insights into the spatial and temporal evolution of climate change impacts and highlight the necessity of region-specific adaptation strategies.

1. Introduction

The IPCC (2023) report indicates a persistent increase in global temperatures over the past century, with 2023 being the warmest year on record since 1850 (Lindsey and Dahlman 2024. This rise in temperatures has led to extreme weather events and significant socio-economic impacts across all inhabited continents (Huang et al 2016, 2017, Herring et al 2021). Notable events include severe floods (Trenberth et al 2015, Zhang et al 2023, Wang et al 2024b), tropical cyclones (Patricola and Wehner 2018)), instances of extreme heat and drought (Diffenbaugh and Field 2013, Dai 2013, Trenberth et al 2015), and increased wildfires (Jolly et al 2015, Williams et al 2019). Understanding the spatial and temporal variability of climate change impacts is crucial for addressing vulnerabilities in different regions and accurately assessing sectoral risks. In this regard, the concept of 'hotspots' has emerged as a valuable tool for identifying areas particularly susceptible to climate change.

The term 'climate change hotspots' was first introduced by Giorgi (2006), defining these areas as those significantly affected by environmental changes or particularly sensitive to global shifts. Hotspots are typically assessed by comparing relative climate changes across two fixed time periods. Research employing the Regional Climate Change Index identified the Mediterranean and Northeast Europe as prominent hotspots when comparing climate responses between 2080-2099 and 1960-1979. However, this method only measures the degree of climate response in specific regions without quantifying climate change at finer geographic scales. Further developments in hotspot identification were made by Williams et al (2007), who utilized standard Euclidean distance (SED) to quantify climate differences between two periods based on average temperature and precipitation changes in winter and summer. This approach allows for the comparison of various meteorological elements and quantifies multiple factors into a single index. Diffenbaugh

et al (2008) applied SED to pinpoint climate change hotspots in the United States, taking into account temperature, precipitation, average changes, and interannual variability during dry and wet seasons, using a baseline from 1961-1989. Building on this, Diffenbaugh and Giorgi (2008) refined the hotspot identification method for a global perspective, incorporating average changes in temperature and precipitation, interannual variability, and extreme conditions across all seasons, establishing hotspot areas under different emission scenarios for the 21st century (baseline period: 1986-2005). The iterative improvements made by these researchers have resulted in a widely adopted method for identifying climate change hotspots, with much of the subsequent research relying on the framework and meteorological factors proposed by Diffenbaugh and Giorgi (2008).

Research has since identified global climate change hotspots using multidimensional climate metrics across various time periods. For instance, Turco et al (2015) analyzed observational data from 1981 to 2010, revealing significant hotspots in the Amazon, Sahel, tropical West Africa, Indonesia, and Central and East Asia. Additionally, numerous studies have utilized datasets from the Coupled Model Intercomparison Project (CMIP) to forecast future climate change hotspots. Diffenbaugh et al (2008) employed CMIP3 data to project future hotspots in the United States under different emission scenarios, identifying the southwestern United States and northern Mexico as the most persistent areas of concern. Expanding on this, Diffenbaugh and Giorgi (2012) used CMIP5 data to estimate global hotspots for the early, middle, and late 21st century, focusing on RCP8.5 and RCP4.5 scenarios. Their analysis identified the Amazon, Sahel, tropical West Africa, Indonesia, and the Qinghai-Tibet Plateau as critical regional hotspots. Ridder et al (2020) provided the first analysis of multiple multivariate compound events (CEs) potentially causing high-impact floods, droughts, and fires, identified hotspots of multivariate CEs including many socio-economically important regions such as North America, Russia and Western Europe. More recently, Fan et al (2021) utilized the latest CMIP6 model data to assess global hotspots under warming scenarios of 1.5 °C, 2 °C, 3 °C, and 4 °C, considering various shared socio-economic pathways (SSP) throughout the 21st century. They found that hotspots in the Amazon, Central and West Africa, Indonesia, and the Qinghai-Tibet Plateau remained consistent across warming levels of 1.5 °C, 2 °C, and 3 °C. Notably, under two scenarios (SSP3-7.0 and SSP5-8.5), regions such as the Arctic, Central America, and Southern Africa are projected to emerge as hotspots by the end of the 21st century with a 4 °C increase in temperature. The CMIP6 model also indicated a higher hotspot index than CMIP5, suggesting a more pronounced cumulative effect of climate change in these newer scenarios.

Initial research on climate change hotspots, conducted by Giorgi (2006), established a baseline period to estimate hotspots for a subsequent period (2080-2099 relative to 1960–1979). In contrast, Diffenbaugh et al (2008) set the baseline to 1961-1989 and assessed climate change hotspots across various emission scenarios over 21 distinct time periods. While this study compared different time periods and emission scenarios, it primarily focused on the differences in hotspot distribution rather than tracking continuous changes in these areas. Subsequent studies continued to select fixed observation periods as baselines. For instance, Diffenbaugh and Giorgi (2008) used 1986-2005 as a baseline to estimate global climate hotspots for the early, middle, and late 21st century. Similarly, Fan et al (2021) analyzed global hotspots for the 21st century under different SSP associated with temperature increases of 1.5 °C, 2 °C, 3 °C, and 4 °C, using 1995–2014 as their baseline. Turco et al (2015) also selected 1951-1980 as a baseline to examine the distribution of climate change hotspots from 1981 to 2010. Although these studies employed fixed reference periods to compare and analyze hotspot distribution, they did not investigate the evolutionary characteristics of SEDs in both hotspot and non-hotspot areas.

In response to the issues identified, this article establishes a benchmark period of 30 years, starting from 1901 and extending to 2020, resulting in a total of 90 research periods. Each period allows for the assessment of global climate change hotspot distribution patterns and the quantitative indices for each land grid point. By analyzing the results across these 90 periods, we can identify trends in hotspot indices. Traditional linear trend methods often rely on arbitrary time intervals, which can obscure significant changes. To overcome these limitations, we employ the ensemble empirical mode decomposition (EEMD) method to explore the nonlinear evolution of hotspot indices across the research periods. Additionally, the contribution of various climate variables to the hotspot index has not been thoroughly quantified. To address this, we employ the geographical detector model (GDM) to quantify the contributions of critical influencing factors behind climate change hotspots. Section 2 outlines the datasets, and methods used for hotspot identification and factor detection. Section 3 presents and discusses the main results, while section 4 offers concluding observations and insights for future research.

2. Data and methods

2.1. Data

This study utilized the CRU TS v4 dataset (Version 4 of the Climatic Research Unit gridded Time Series), which offers climate data for all land areas worldwide,

excluding Antarctica. This dataset is based on an extensive network of meteorological stations and produces climate data on a $0.5^{\circ} \times 0.5^{\circ}$ latitude and longitude grid through interpolation methods. The primary climate variables analyzed in this study were temperature and precipitation (monthly, spanning January 1901 to December 2022). The strengths of the CRU TS dataset, including the continuity of its time series and comprehensive global coverage, facilitate reliable quantitative analysis of large-scale climate change. Harris et al (2020) provided a thorough overview of the updates and enhancements made to the CRU TS v4 dataset, particularly regarding data processing and calibration. Furthermore, comparisons with other high-resolution datasets have confirmed the global reliability of CRU TS v4.

2.2. Identification of climate change hotspots

Previous studies have developed refined methods for identifying climate change hotspots, particularly under extreme weather conditions. Examples include research on extreme precipitation hotspots (Xu et al 2021a), extreme climate hotspots (Xu et al 2019), and the approaches proposed by Diffenbaugh and Giorgi (2012). In this study, we adopt the SED method introduced by (Diffenbaugh and Giorgi 2012) to quantify overall climate change. We selected seven climate indicators for each of the four seasons—December-January-February, March-April-May, June-July-August, and September-October-November—to identify global climate change hotspots from 1901 to 2021. These indicators include the average values, interannual variability, and extreme values of temperature and precipitation. The SED (a unitless measure) aggregates changes in these indicators between various time periods and a baseline period (1901–1930) based on observational data. The spatial patterns of average climate indicators during the baseline period are shown in figures S1 and S2. At each land grid point, the total SED is calculated as follows:

$$SED_t = \sqrt{\sum_{\nu} SED_{t,\nu}}$$
 (1)

for,

$$SED_{t,v} = (x_{tv} - x_{bv})^2 / \left\{ \max_{(i,j)} \left[abs(x_{tv} - x_{bv}) \right] \right\}^2$$
 (2)

where x_{tv} denotes the value of climate indicator v during the study period, x_{bv} denotes the value of variable v in the 'baseline' period, and $\max[abs(x_{tv}_x_{bv})]_{ij}$ refers to the maximum absolute change in indicator v across all land grid points (for longitudes i[0,360] and latitudes j[0,180]). The baseline period spans 1901–1930, while the study period begins in 1902–1931 and advances in one-year increments, forming a sliding 30 year window. This process results in 90 study periods, ending with 1991–2020. Each study

period (t[1,90]) defines x_{ft} and $SED_{t,v}$ as functions of t. The $SED_{t,v}$ calculation incorporates seven climate indicators: The absolute change in mean temperature (ΔT) directly quantifies surface temperature variations and serves as a fundamental indicator of global warming trends. Precipitation alteration constitutes a critical component of hydrological cycle evolution, where the relative change in mean precipitation (ΔP) reflects water resource availability shifts at regional and global scales, exerting substantial impacts on ecosystems and agricultural systems. The detrended temperature standard deviation ($\Delta T_{\rm var}$) captures interannual temperature variability and anomalous fluctuations, revealing inherent climate system instability and its responses to extreme events. The relative change in precipitation coefficient of variation ($\Delta P_{\rm var}$) quantifies interannual precipitation uncertainty and extremality, indicative of drought or deluge frequency alterations. The frequency of years exceeding baseline maximum temperatures (F_{hot}) directly measures extreme heat event occurrence, critical for heatwave risk assessment. The frequency of years below baseline minimum precipitation (F_{drv}) characterizes drought event recurrence, reflecting extreme deviations in water resource availability. The frequency of years surpassing baseline maximum precipitation (Fwet) tracks extreme precipitation events, crucial for flood risk evaluation. Collectively, these seven indicators encompass three primary dimensions of climate change: mean state $(\Delta T, \Delta P)$, variability $(\Delta T_{\text{var}}, \Delta P_{\text{var}})$, and extremes $(F_{hot}, F_{dry}, F_{wet})$ —all critical factors influencing ecosystems, agricultural productivity, infrastructure resilience, and public health.

The seasonal stratification of meteorological variables into winter, spring, summer, and autumn accounts for distinct seasonal climatic characteristics driven by solar radiation patterns, atmospheric circulation regimes, and precipitation seasonality. This temporal partitioning enhances analytical precision by isolating seasonal climate signals, mitigating data aggregation biases arising from inter-seasonal variability, and facilitating targeted interpretation of seasonal climate dynamics. Furthermore, seasonal classification aligns with international climatological research conventions, enabling cross-study comparisons and supporting multi-source data integration to enhance methodological robustness and generalizability. Seasonal-scale analysis additionally identifies climate-sensitive regions and temporal vulnerabilities, providing critical insights for developing seasonspecific adaptation strategies.

This integrated approach captures multidimensional characteristics of temperature and precipitation dynamics across temporal scales, ensuring the SED index effectively represents climate change complexity and regional heterogeneity. Concurrently, seasonal classification reveals differential climate change manifestations across seasons, circumventing potential masking effects inherent in annual averaging while enhancing analytical specificity.

2.3. Definition of nonlinear trend

The method we use to derive the long-term trend of global SED is multidimensional EEMD (MEEMD; Wu et al 2009). MEEMD is an extension of the (EEMD; Huang et al 1998, Huang and Wu 2008, Wu and Huang 2009), which is a local and adaptive analysis of nonlinear and non-stationary time series. Both EEMD and MEEMD have been widely applied in climate research (Qian et al 2010, Cheng et al 2017). EEMD decomposes a time series, x(t), into a set of amplitude-frequency-modulated oscillatory components (intrinsic mode functions) $C_i(t)$, i = 1,2,...n and a residual R(t), allowing the separation of signals at different timescales, such as the annual cycle, interannual variability, decadal trends, multidecadal variations, and secular trends, as demonstrated in figure S3.

$$x(t) = \sum_{j=1}^{n} c_j(t) + R(t).$$
 (3)

In this study, we focus on the long-term trend of global SED, represents by R(t), which is defined as a curve that is either monotonic or contains only one extremum, from which no additional oscillatory components can be extracted (Wu et al 2007). The time-varying nature of this intrinsic trend offers a novel perspective on trend analysis. Following Ji et al (2014), we define the nonlinear trend of a SED series as Trend(t) = R(t)-R(1), t = 1,2... 90, representing the accumulated change in SED from present. The rate of nonlinear change can then be calculated by determining the slope of the trend at any given point in time, which varies across both time and space. This approach allows us to quantify the magnitude and spatial distribution of the changing rate of SED. The instantaneous rate of change is calculated as the temporal derivatives of the nonlinear trend. For example, the rate of change at 1910 is calculated as (Trend at 1911-1909)/2.

For a multidimensional spatial–temporal dataset, we piece together R(t)s values from all grid points to generate a comprehensive representation of the evolution of SED's long-term trends. This approach, which accounts for spatial and temporal variability, provides a more detailed understanding of how climate change hotspots respond to global warming over a century, compared to the traditional linear, time-invariant methods.

2.4. Assessing critical influencing factors

To analyze the contribution of meteorological factors to changes in hotspot distribution, we use the Geodetector Method (GDM) to quantify the spatial heterogeneity of each factor with respect to the SED distribution. The GDM method has been widely

applied across disciplines such as health, ecology, geography, and atmospheric studies (Hu et al 2021, Luo et al 2016, Yin et al 2019, Zhao et al 2020), demonstrating robust performance. Specifically, we adopt the q-statistic proposed by Wang et al (2010, 2016) to calculate spatial heterogeneity and the k-means clustering method used in Zhao et al (2020) for factor grouping. In this analysis, each time window serves as the study unit. For the 90 time periods, we calculate the contribution of seven meteorological factors for each period. The annual value of each meteorological factor is computed as the sum of its values across all four seasons. Using this approach, we derive the O value for each factor in each period, ranging from 0 to 1. A larger Q value indicates stronger spatial heterogeneity and a greater contribution of the meteorological factor to the SED distribution. Conversely, a smaller Q value reflects weaker spatial heterogeneity and a lower contribution. The calculation formula for O is as follows:

$$q_{x_t} = 1 - \frac{\sum_{i=1}^{m} N_i \sigma_i^2}{N\sigma^2}.$$
 (4)

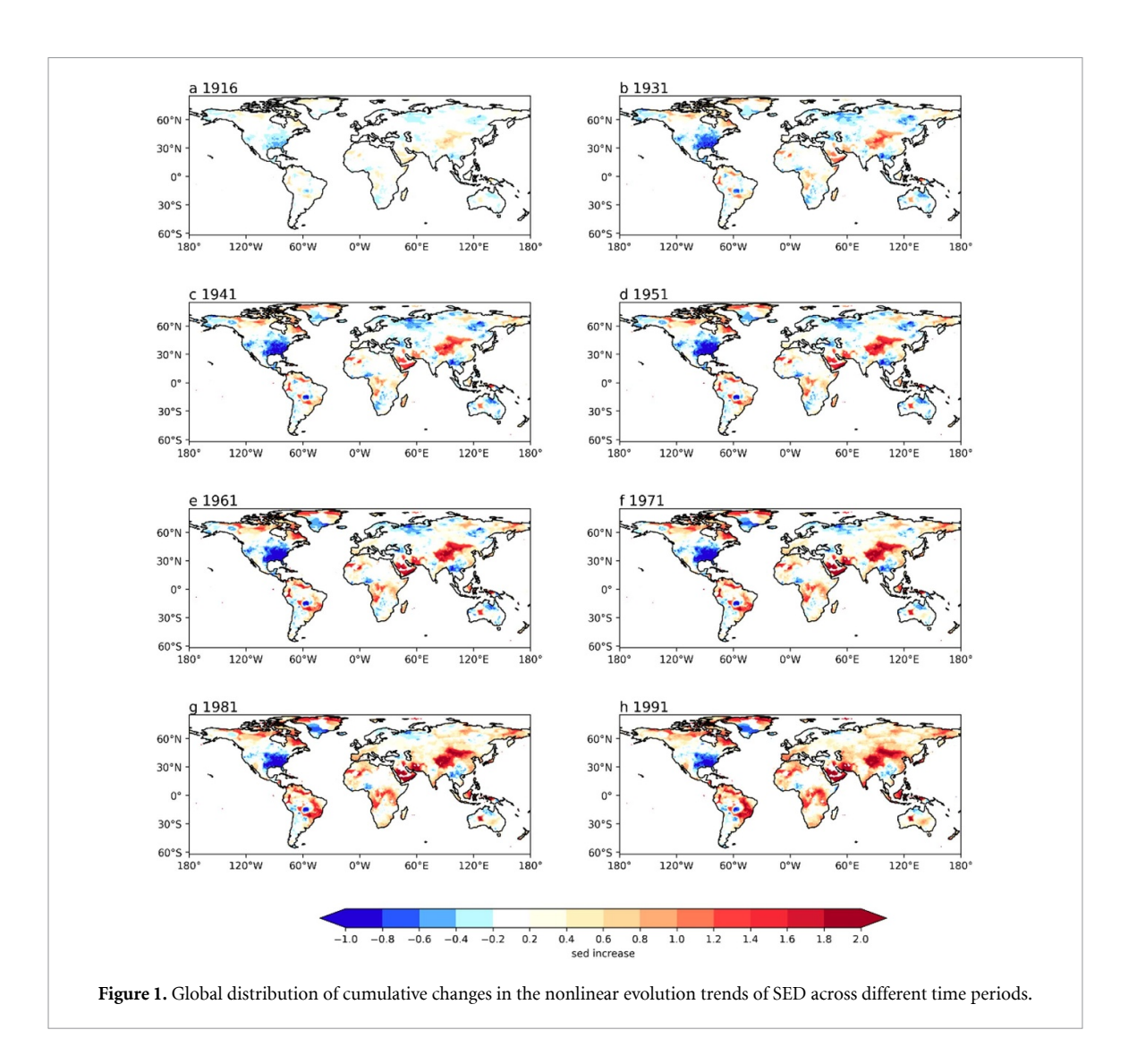
Among them, q_{x_t} represents the contribution of meteorological factor x to SED during the research period t. m represents the number of layers into which meteorological factor x_t is divided using K-means (m=2,3,4,...). N_i denotes the number of grid points for meteorological factor x_t in layer i, and σ_i^2 represents the variance of x_t in layer i. N signifies the total number of global grid points for x_t , and σ^2 denotes the global variance of x_t .

It is important to note that the Geographical Detector Model (GDM) is designed to quantify spatial stratified heterogeneity and assess the strength of associations between variables. However, GDM does not provide evidence of causality; it only indicates the influence of various factors on the observed spatial patterns.

3. Results

3.1. Evolution of global climate change hotspots

To enhance our understanding of climate change hotspots, we build on existing research and hotspot definitions, noting that most studies emphasize comparisons of specific periods against a baseline under various scenarios. While insightful, such approaches often overlook intermediate processes that shape final outcomes. Key questions remain largely unanswered: Which regions exhibit the earliest responses to climate change? How does hotspot intensity evolve within the same region over time? Addressing these questions is essential for a fuller understanding of climate dynamics and how responses may spread and intensify. Therefore, we employed a sliding window method to construct a dynamic time series of hotspot indices, enabling us to observe shifts in intensity and spatial spread. We also utilized the



EEMD method to explore the long-term evolutionary characteristics of these trends. This approach has been effective in detecting patterns in other climate system aspects, such as global land and sea surface temperature trend (Ji et al 2014, Xu et al 2021b), global vegetation (Pan et al 2018), and drying and wetting trends in China (Wu et al 2024). By integrating these methods, we provide a temporal perspective on climate impacts, revealing how climate change hotspots may shift and expand over time

According to the methodology and definitions previously mentioned, we obtained a time series of SED values spanning a period of 90 years for each grid point. Here, SED (1) represents the hotspot index calculated for 1902–1931 relative to the baseline period, which, for convenience, we refer to as the hotspot index in 1902. Similarly, SED (90) is for 1991–2020 relative to the baseline period. By applying EEMD method to the hotspot index at each grid point, we can extract the final component representing the long-term trend, allowing us to piece together a comprehensive spatial—temporal evolution of the global climate change hotspot index. This is the essence of

the MEEMD, with more details were introduced by Ji *et al* (2014).

The spatial evolution of accumulated changes over time is depicted in figure 1, revealing pronounced regional heterogeneity in trends. In the earliest period (figure 1(a)), areas exhibiting substantial SED changes are relatively limited, with most regions showing near-zero values, indicating minimal deviation from baseline climate sensitivity. Subtle increases first appear over the Tibetan Plateau and Mongolia, with smaller isolated patches emerging in northern North America, South America, highlatitude regions of Canada and Greenland, and Africa. Conversely, regions such as the southeastern United States, north-central Eurasia, southwestern China, and Australia exhibit slight decreases, suggesting initial zones of reduced sensitivity to climatic changes. This general pattern persists over subsequent decades, but the intensity and spatial extent of changes begin to increase (figure 1(b)). By 1941 (figure 1(c)), areas experiencing both increases and decreases become more defined, with their magnitudes growing noticeably. The Tibetan Plateau, Mongolia, high-latitude regions of Canada and Greenland, and the Arabian

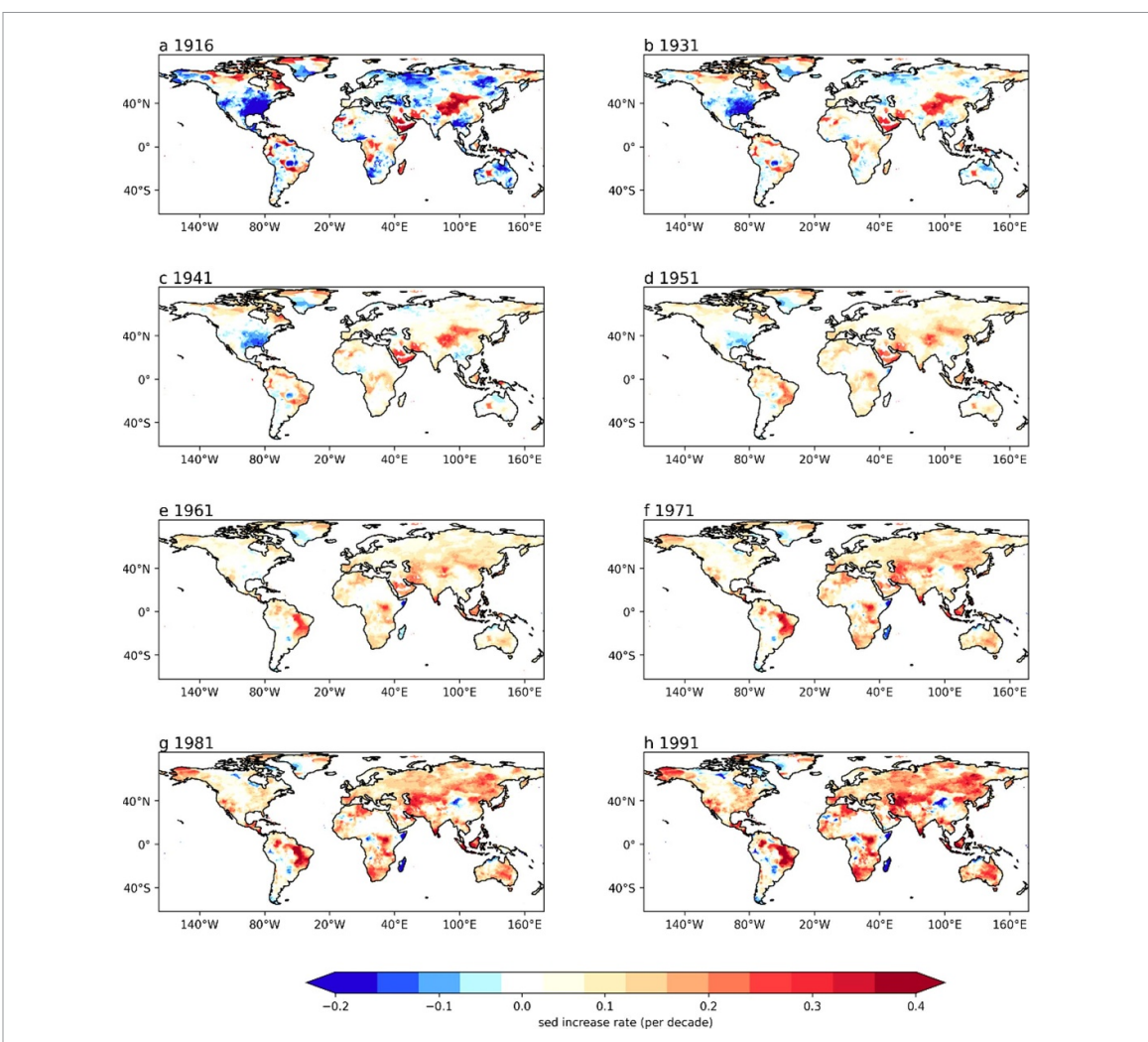


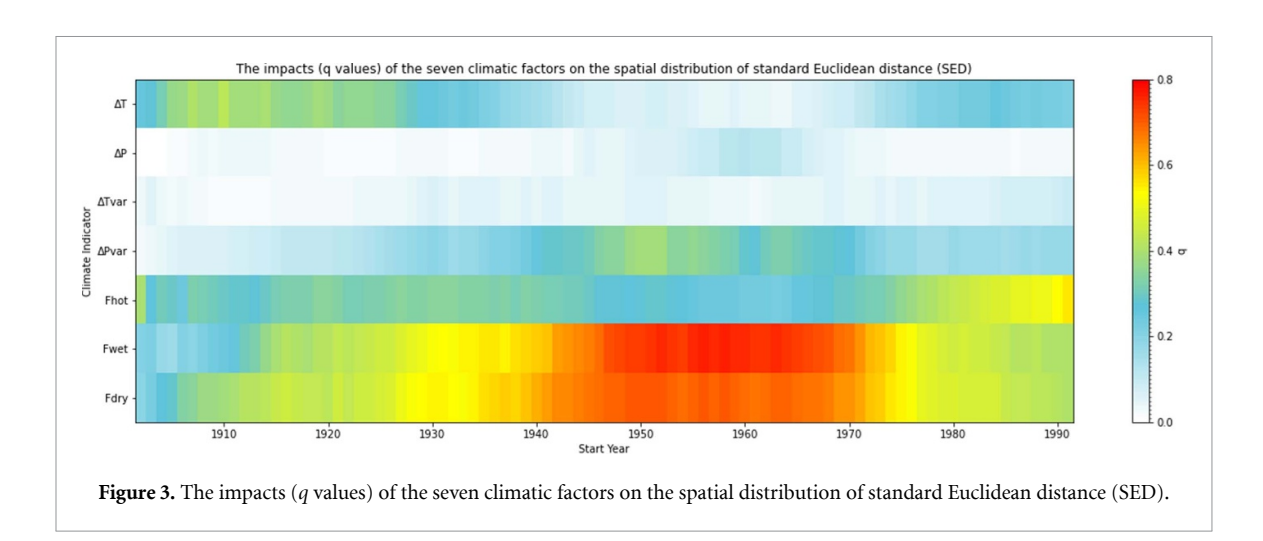
Figure 2. Global distribution of instantaneous rate of change (every decade) of nonlinear evolution trend of SED in different time periods.

Peninsula increasingly dominate as hotspots of rising sensitivity, while regions of decline—including the southeastern United States, north-central Eurasia, and southwestern China-continue to expand and intensify. By 1951 (figure 1(d)), the spatial contrast between regions of increasing and decreasing sensitivity becomes sharper, reflecting diverging regional responses to climate forcing. From 1961 onward, the patterns observed earlier remain consistent, albeit with a gradual spatial expansion of areas experiencing increases and a contraction of regions showing decreases (figures 1(e)–(g)). These decades mark a transitional phase, during which hotspots of increasing sensitivity become more spatially coherent, signifying a shift toward more widespread and pronounced regional trends. The final frame, 1991 (figure 1(h)), represents the culmination of nearly a century of evolving climate sensitivity. Regions such as the Tibetan Plateau, Mongolia, and the Arabian Peninsula, which initially exhibited subtle increases, now show dramatic and widespread rises in SED. Additionally, parts of Africa and South America reveal

significant positive trends, while much of Eurasia displays heightened sensitivity. In contrast, the southeastern United States and southwestern China remain prominent as regions of persistently low sensitivity, reflecting entrenched resistance to the trends observed elsewhere. However, this evolution of the SED trends cannot be revealed by the linear trend (figure S5a).

3.2. Evolution of global climate hotspots change rates

Given the time-varying nature of the SED trends, their temporal rates of change-calculated as the temporal derivatives of the non-linear trends at specific years-provide valuable insight into the pace and direction of these changes. These rates, representing the slope of the non-linear trend at each year, offer a complementary perspective to figure 1 by emphasizing the dynamic evolution of SED trends over time. During the early decades, the rates of change in SED trends exhibit pronounced regional contrasts (figures 2(a)–(d)). Negative rates dominate



in the northern high latitudes (e.g. Eurasia and North America, except for the high-latitude regions of Canada and Greenland) and the southern extratropics, reflecting a rapid decline in SED trends in these areas. Conversely, positive rates emerge prominently in the tropics and subtropics, particularly over regions such as the Tibetan Plateau, Mongolia, and the Arabian Peninsula, signaling an acceleration of SED trends. Over time, these spatial patterns begin to evolve. The regions with negative rates (blue areas) contract rapidly, while the regions with positive rates (red areas) expand. By 1951, areas with declining SED trends become increasingly confined, primarily to southern Greenland, southeastern North America, and a few isolated locations. This spatial contraction indicates that the rate of SED trend decline in southeastern North America is slowing, while in Eurasia, the SED trends have already transitioned from a declining phase to an upward trajectory. Simultaneously, regions such as the Tibetan Plateau and Mongolia, which previously experienced accelerated increases in SED trends, show a slowing rate of growth, reflecting an early shift in their dynamic evolution.

After 1961, a significant transition occurs in the global patterns of SED trend rates. The southeastern North American continent, which had previously shown declining SED trends, experiences a turnaround, with its rates shifting to positive values. In contrast, regions like the Tibetan Plateau and Mongolia experience a continued deceleration in SED growth rates, highlighting the complex interplay of regional climatic factors and internal variability. During this period, the global landmasses begin to exhibit a more unified characteristic: a widespread acceleration in SED increases, as indicated by the dominance of positive rates across most regions. This shift underscores a global-scale intensification in SED trends driven by both anthropogenic forcing and natural variability. By the end of the study period, the SED growth rates reach their highest levels, with the most pronounced increases concentrated in the mid-to-high latitudes of Eurasia and across much of the Southern Hemisphere. These regions emerge as global hotspots for accelerated SED trends, reflecting the combined effects of intensifying anthropogenic impacts and regional climate feedback mechanisms. However, this evolution of the SED trend rates also cannot be reflected by the straight line fitting (figure S5(b)).

3.3. Climatic factors influencing the spatial distribution of SED

To systematically analyze the spatial-temporal characteristics of climate change hotspots, we quantified the relative contributions of seven climatic indicators, encompassing both temperature and precipitation factors, to the spatial distribution of SEDs using the Geographical Detector Model (GDM). Figure 3 reveals the temporal evolution of these contributions, providing critical insights into the changing influencing factors of hotspot formation. We employed the significance test method for the statistic q described by Wang et al (2016) to assess our results. The findings indicate that, except for ΔT_{var} and ΔP_{var} , the q values for other factors—such as mean temperature change, extreme precipitation, and extreme high temperature—are statistically significant. During the early decades, the spatial distribution of climate change hotspots was predominantly influenced by shifts in the mean surface temperature (ΔT). Elevated q-values for ΔT suggest that gradual changes in average temperature were the primary factor shaping hotspot formation, reflecting the initial stages of global warming, where the impacts of rising mean temperatures on regional climates were relatively uniform and widespread. However, a notable transition occurred after 1920, when precipitation-related extremes, specifically the frequency of extreme wet events (F_{wet}) and drought years (F_{dry}), emerged as dominant contributors. During 1940 and 1970, the q-values for F_{wet} and F_{drv} reached their peak, highlighting the critical role of spatial variability in extreme precipitation events in influencing hotspots. Concurrently,

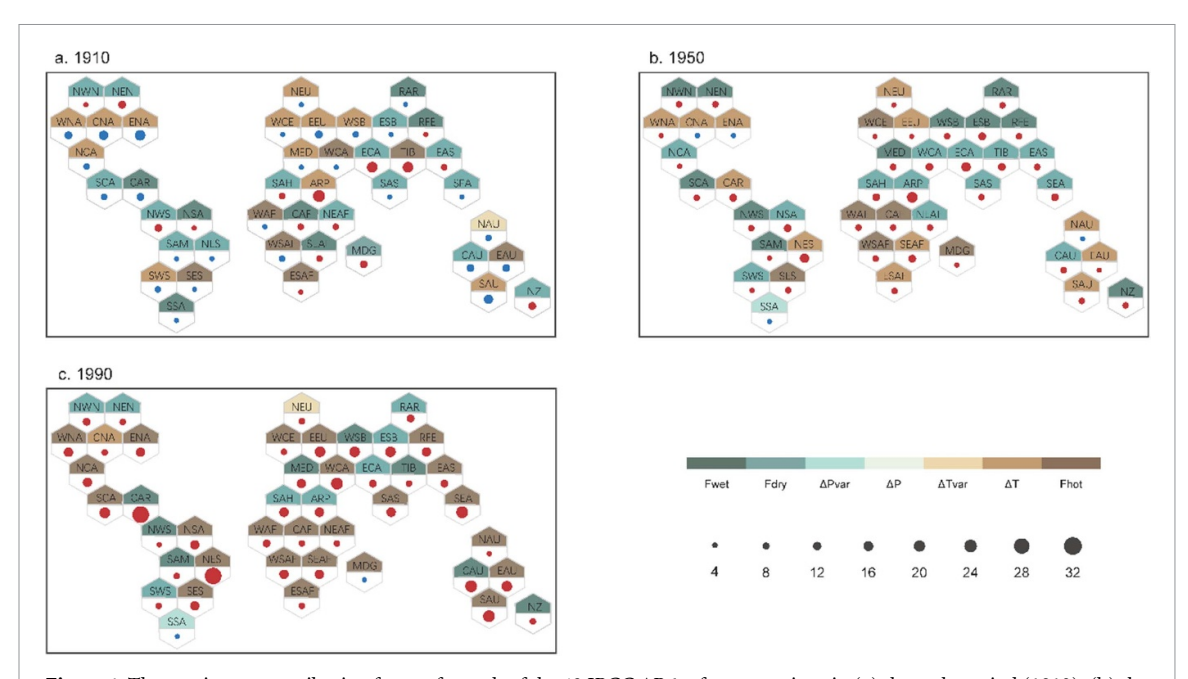


Figure 4. The maximum contributing factors for each of the 43 IPCC AR6 reference regions in (a) the early period (1910), (b) the mid-term (1950), and (c) the later period (1990). Colors in the graph indicate the meteorological factors with the greatest contribution to the SED distribution in the region during that time. Solid dots represent the instantaneous rates of cumulative trends in SED in the region during this period. Blue indicates negative values, while red indicates positive values.

the influence of precipitation variability (ΔP_{var}) increased moderately, further underscoring the significance of fluctuating precipitation patterns during this phase. In contrast, temperature-related indicators, including ΔT and its variability (ΔT_{var}), exhibited a marked decline in their q-values, indicating a reduced influence of mean temperature changes and temperature variability on hotspot distributions. This shift aligns with observed trends in global mean temperature, which exhibited a cooling phase during this period. After 1970, the landscape of climate change influencing factors underwent another significant shift. The influence of precipitation-related extremes began to diminish, as evidenced by their gradually declining q-values, although they remained substantial. Simultaneously, the frequency of extreme heat events (F_{hot}) rose to prominence, with steadily increasing q-values over time. This transition reflects the escalating impact of high-temperature extremes, such as heatwaves, as a defining characteristic of contemporary climate hotspots. At the end, Fhot had become the most influential indicator, signifying a paradigm shift in hotspot formation mechanisms from precipitation-related extremes to temperature-related impacts, influenced by continued global warming.

To further analyze the temporal evolution of climate change hotspots, we assessed the dominant contributing factors across global regions as defined by the IPCC AR6 WGI (Iturbide *et al* 2020). Figure 4 illustrates the primary climatic factors influencing hotspots for three representative periods (1910, 1950, and 1990). In 1910, changes in mean surface temperature (ΔT) dominated across 37.21% (table S1)

of global land regions, particularly in high-latitude areas such as Northern Europe and North America. Precipitation-related extremes also contributed significantly, with wet events (F_{wet} , 13.95%) and dry extremes (F_{dry} , 32.56%) being prominent in tropical regions and eastern Asia. By 1950, precipitationrelated extremes became increasingly influential, signaling a shift in the factors influencing hotspot. Dry extremes (F_{dry} , 30.23%) emerged as the dominant factor in regions such as South and East Asia and northern Africa, reflecting heightened susceptibility to drought conditions. Concurrently, wet extremes (F_{wet} , 25.58%) became more prominent in areas like Siberia, Mediterranean, and high-latitude regions of Canada and Greenland, emphasizing the growing impact of extreme precipitation events. This period marked a significant decline in the influence of temperature-related indicators such as ΔT , corresponding to observed global cooling trends during this time. By 1990, heat extremes (F_{hot}) had become the most influential factor, dominating 41.86% of global land regions. This factor was particularly impactful in North America, Eastern South America, Central Europe, Africa, East Asia, and Australia, underscoring the intensifying role of heatwaves under accelerating global warming. Despite this shift, precipitationrelated extremes (F_{drv} and F_{wet}) continued to account for 51.16% of hotspot influencing factors, highlighting the enduring influence of hydrological extremes.

The lower portion of each hexagon provides a nuanced representation of the averaged SED trend rates. The color indicates whether the trend is increasing (red) or decreasing (blue), while the size of the dots reflects the absolute rate of change, with larger

dots signifying more pronounced shifts. During the early period, blue dots are predominant across many regions, signifying a general decline in the intensity of climate change hotspots. The variability in dot size highlights regional differences: while some areas experienced only minor decreases, others, such as parts of North America, exhibited more substantial declines. In contrast, certain regions, including the Tibetan Plateau, eastern Central Asia, and the Arabian Peninsula, emerged as areas of rapid increase, marked by red dots of moderate size. These regions foreshadow the future intensification of climate change impacts, influenced by localized factors such as temperature and precipitation extremes. By 1950, the spatial distribution of trends undergoes a notable shift. Most regions begin to exhibit increasing trends, as indicated by the growing prevalence of red dots. Notably, regions such as Europe, Siberia, and parts of East Asia experience moderate to large increases in hotspot intensity, suggesting a transition to accelerated climate change impacts. Simultaneously, the southeastern part of North America shows a diminishing rate of decline, with smaller blue dots indicating a tapering downward trend. This period reflects a dynamic phase of regional divergence, where hotspots in certain areas begin to intensify while others stabilize or show muted changes. By 1990, red dots dominate the global landscape, illustrating a widespread and rapid intensification of climate change hotspots. Lots regions stand out with large red dots, indicating significant increases in the rate of change. Only a few regions, such as the southern part of the South American and Madagascar, exhibit weak declines, as marked by small blue dots. These isolated exceptions highlight localized factors that may temporarily counterbalance broader global trends. Overall, the spatial pattern underscores a near-universal shift toward accelerating climate change impacts by the latest period.

It is important to note that while our study primarily focuses on meteorological indicators (temperature, precipitation, and their extremes) to identify climate change hotspots, this approach may oversimplify the complexity of climate forcing. External forcing factors such as greenhouse gas concentrations, aerosols, and land use changes, as well as ocean—atmosphere interactions and teleconnection processes (e.g. ENSO, AMO, IOD), are also key drivers of climate variability. Although our preliminary analysis of large-scale climate modes (e.g. the relationships between AMO/PDO and the SED index) suggests that oceanic signals can modulate regional climate patterns, the underlying physical mechanisms remain to be fully elucidated.

4. Conclusions and discussion

This study introduces the dynamical climate change hotspots index SED, derived from seasonal variations in average temperature and precipitation, interannual variability, and extreme values. The evolution of the nonlinear long-term trends in the SED was analyzed using EEMD. The results reveal a marked spatial variability in SED trends globally, with distinct regional disparities. Over time, regions near the Tibetan Plateau, Mongolia, and the Arabian Peninsula consistently exhibit increasing SED values, becoming prominent hotspots of global climate sensitivity. Conversely, the southeastern United States and southwestern China show a declining SED trend during the early decades, maintaining a status of low sensitivity. Most other regions, however, have experienced a shift toward rising SED in later periods.

Regions such as the Tibetan Plateau and Mongolia, which initially displayed increases in SED, demonstrate a rapid response to global warming, as noted in previous studies (Yao et al 2000, Batima et al 2005, Lu et al 2009). Despite a deceleration in the rate of SED growth, the accumulated effects have led to significant climate-related challenges in these areas (You et al 2021, Zhou and Zhang 2021, Meng et al 2023). The southeastern United States, characterized by a prominent 'warming hole' (Meehl et al 2012, Eischeid et al 2023), shows a marked decline in SED. Yet, the contraction of this cooling zone and the subsequent shift toward increased sensitivity indicate growing vulnerability to extreme weather events (Eck et al 2020, Takhellambam et al 2023). Globally, the overall acceleration in SED trends signals that the impacts of climate change are expanding, rather than remaining confined to specific regions. Kornhuber et al (2024) also document this shift, noting the increasing frequency of extreme heatwaves across every continent except Antarctica, which have become widespread, intense, and persistent.

The latitude-time evolution of SED, along with the rates of change in SED trends, reveals distinct trajectories for the two hemispheres. The Western Hemisphere exhibits a more heterogeneous response, with regions of both increasing and decreasing trends, particularly in the mid-latitudes. In contrast, the Eastern Hemisphere shows more uniform increases in SED, with hotspots of sensitivity intensifying in the Tibetan Plateau and Arabian Peninsula. These hemispheric differences likely arise from a complex interplay of regional climate dynamics, land-ocean distribution, and anthropogenic influences. They underscore the region-specific responses to both internal variability and external forcing, offering

crucial insights into the hemispheric asymmetries in the evolution of climate change hotspots.

The temporal shift in the key influencing factors of climate change hotspots further emphasizes the evolving nature of climate change impacts. Initially, gradual temperature increases dominated hotspot formation, but over time, more localized and extreme climate events have become the primary influencing factors. This transition reflects the growing role of extreme weather in shaping spatial variability in climate change impacts, a trend that is corroborated by the rising frequency of such events globally (Robinson et al 2021, Duan et al 2024, Lyu et al 2024, Tian et al 2024, Wang et al 2024a, Zhang et al 2024). Regions facing frequent extreme events, such as droughts, floods, and heatwaves, are increasingly becoming focal points of climate-induced stress. These developments carry profound implications for ecosystems, agriculture, and socio-economic systems, highlighting the urgent need for targeted mitigation and adaptation strategies.

Data availability statement

The data that support the findings of this study are openly available at the following URL/DOI: https://crudata.uea.ac.uk/cru/data/hrg/cru_ts_4.08/.

Acknowledgments

This work was jointly supported by the Joint Funds of the National Natural Science Foundation of China (U2342205), National Natural Science Foundation of China (42494871 and 42275034), and Gansu Provincial Science and Technology Project (23JRRA1030).

Conflict of interest

The authors declare that they have no known competing financial interests or personal relationships that could have appeared to influence the work reported in this paper.

CRediT authorship contribution statement

Du Zhuoya: Writing—review & editing, Writing—original draft, Visualization, Validation, Software, Methodology, Investigation, Formal analysis, Data curation, Conceptualization. Han Xuchou: Writing—review & editing, Visualization, Software, Methodology, Conceptualization. Ji Fei: Writing—review & editing, Writing—original draft, Validation, Supervision, Resources, Methodology, Funding acquisition, Formal analysis, Conceptualization. Xu Zhenhao: Writing—review & editing, Supervision. Guan Xiaodan: Writing—review & editing,

Supervision. **Huang Jianping:** Writing—review & editing, Supervision.

ORCID iDs

Xuchou Han https://orcid.org/0009-0004-3861-9762

Fei Ji https://orcid.org/0000-0002-7985-1558 Zhenhao Xu https://orcid.org/0000-0001-5997-7439

Jianping Huang https://orcid.org/0000-0003-2845-797X

References

Batima P, Natsagdorj L, Gombluudev P and Erdenetsetseg B 2005 Observed climate change in Mongolia (AIACC WP No. 12). assessments of impacts and adaptations to climate change (AIACC) project (available at: www.aiaccproject.org)

Cheng S, Huang J, Ji F and Lin L 2017 Uncertainties of soil moisture in historical simulations and future projections *J. Geophys. Res.* 122 2239–53

Dai A 2013 Increasing drought under global warming in observations and models *Nat. Clim. Change* 3 52–58

Diffenbaugh N S and Field C B 2013 Changes in ecologically critical terrestrial climate conditions *Science* 341 486–92

Diffenbaugh N S and Giorgi F 2012 Climate change hotspots in the CMIP5 global climate model ensemble *Clim. Change* 114 813–22

Diffenbaugh N S, Giorgi F and Pal J S 2008 Climate change hotspots in the United States *Geophys. Res. Lett.* **35** L16709

Duan R, Huang G, Wang F, Tian C and Wu X 2024 Observations over a century underscore an increasing likelihood of compound dry-hot events in China *Earth's Future* 12 e2024EF004546

Eck M A, Murray A R, Ward A R and Konrad C E 2020 Influence of growing season temperature and precipitation anomalies on crop yield in the southeastern United States *Agric. For. Meteorol.* **291** 108053

Eischeid J K *et al* 2023 Why has the summertime central U.S. Warming hole not disappeared? *J. Clim.* **36** 7319–36

Fan X, Miao C, Duan Q, Shen C and Wu Y 2021 Future climate change hotspots under different 21st century warming scenarios *Earth's Future* 9 e2021EF002027

Giorgi F 2006 Climate change hot-spots *Geophys. Res. Lett.* **33** Harris I, Osborn T J, Jones P and Lister D 2020 Version 4 of the CRU TS monthly high-resolution gridded multivariate climate dataset [dataset] *Sci. Data* **7** 109

Herring S C, Christidis N, Hoell A, Hoerling M P and Stott P A 2021 Explaining extreme events of 2019 from a climate perspective *Bull. Am. Meteorol. Soc.* 102 S1–S115

Hu M *et al* 2021 Risk of coronavirus disease 2019 transmission in train passengers: an epidemiological and modeling study *Clin. Infect. Dis.* **72** 604–10

Huang J, Yu H, Dai A, Wei Y and Kang L 2017 Drylands face potential threat under 2 °C global warming target *Nat. Clim. Change* 7 417–22

Huang J, Yu H, Guan X, Wang G and Guo R 2016 Accelerated dryland expansion under climate change *Nat. Clim. Change* 6 166–72

Huang N E and Wu Z 2008 A review on Hilbert–Huang transform: the method and its applications on geophysical studies *Rev. Geophys.* 46 RG2006

Huang N, Shen Z, Long S, Wu M, Shih H, Zheng Q, Yen N-C, Tung C C and Liu H 1998 The empirical mode decomposition method and the Hilbert spectrum for non-stationary time series analysis *Proc. R. Soc. A* 454 903995

- Iturbide M et al 2020 An update of IPCC climate reference regions for subcontinental analysis of climate model data: definition and aggregated datasets Earth Syst. Sci. Data 12 2959–70
- Ji F, Wu Z, Huang J and Chassignet E P 2014 Evolution of land surface air temperature trend *Nat. Clim. Change* 4 462–6
- Jolly W, Cochrane M, Freeborn P, Holden Z A, Brown T J, Williamson G J and Bowman D M J S 2015 Climate-induced variations in global wildfire danger from 1979 to 2013 Nat. Commun. 6 7537
- Kornhuber K, Bartusek S, Seager R, Schellnhuber H J and Ting M 2024 Global emergence of regional heatwave hotspots outpaces climate model simulations *Proc. Natl Acad. Sci.* USA 121 e2411258121
- Lindsey R and Dahlman L 2024 Climate change: global temperature. NOAA climate.gov. reviewed by J. Blunden (available at: www.energy.gov/sites/default/files/2024-02)
- Lu N, Wilske B, Ni J, John R and Chen J 2009 Climate change in inner Mongolia from 1955 to 2005—trends at regional, biome, and local scales Environ. Res. Lett. 4 045006
- Luo W, Jasiewicz J, Stepinski T, Wang J, Xu C and Cang X 2016 Spatial association between dissection density and environmental factors over the entire conterminous United States Geophys. Res. Lett. 43 692–700
- Lyu Y *et al* 2024 The characterization, mechanism, predictability, and impacts of the unprecedented 2023 Southeast Asia heatwave *npj Clim. Atmos. Sci.* 7 246
- Meehl G A, Arblaster J M and Branstator G 2012 Mechanisms contributing to the warming hole and the consequent U.S. East–West differential of heat extremes *J. Clim.* 25 6394–408
- Meng Y, Duan K, Shi P, Shang W, Li S, Cheng Y, Xing L, Chen R and He J 2023 Sensitive temperature changes on the Tibetan Plateau in response to global warming *Atmos. Res.* 294 106948
- Pan N, Feng X, Fu B, Wang S, Ji F and Pan S 2018 Increasing global vegetation browning hidden in overall vegetation greening: insights from time-varying trends *Remote Sens*. Environ. 214 59–72
- Patricola C M and Wehner M F 2018 Anthropogenic influences on major tropical cyclone events *Nature* **563** 339–46
- Qian C, Wu Z, Fu C B and Zhou T J 2010 On multi-timescale variability of temperature in China in modulated annual cycle reference frame *Adv. Atmos. Sci.* 27 1169–82
- Ridder N N, Pitman A J, Westra S, Ukkola A, Do H X, Bador M, Hirsch A L, Evans J P, Di Luca A and Zscheischler J 2020 Global hotspots for the occurrence of compound events *Nat. Commun.* 11 5956
- Robinson A, Lehmann J, Barriopedro D, Rahmstorf S and Coumou D 2021 Increasing heat and rainfall extremes now far outside the historical climate *npj Clim. Atmos. Sci.* 4 45
- Takhellambam B S, Srivastava P, Lamba J, McGehee R P, Kumar H and Tian D 2023 Projected mid-century rainfall erosivity under climate change over the southeastern United States *Sci. Total Environ.* **865** 161119
- Tian Y, Giaquinto D, Di Capua G, Claassen J N, Ali J, Li H and De Michele C 2024 Historical changes in the causal effect networks of compound hot and dry extremes in central Europe Commun. Earth Environ. 5 764
- Trenberth K, Fasullo J and Shepherd T 2015 Attribution of climate extreme events *Nat. Clim. Change* 5 725–30
- Turco M, Palazzi E, von Hardenberg J and Provenzale A 2015 Observed climate change hotspots *Geophys. Res. Lett.* 42 3521–8

- Wang C, Li Z, Chen Y, Li Y, Ouyang L, Zhu J, Sun F, Song S and Li H 2024a Changes in global heatwave risk and its drivers over one century *Earth's Future* 12 e2024EF004430
- Wang H, Wang S, Shu X, He Y and Huang J 2024b Increasing occurrence of sudden turns from drought to flood over China J. Geophys. Res. 129 e2023JD039974
- Wang J-F, Zhang T-L and Fu B-J 2016 A measure of spatial stratified heterogeneity *Ecol. Indic.* 67 250–6
- Wang J, Li X, Christakos G, Liao Y, Zhang T, Gu X and Zheng X 2010 Geographical detectors-based health risk assessment and its application in the neural tube defects study of the Heshun region, China *Int. J. Geogr. Inf. Sci.* 24 107–27
- Williams A P, Abatzoglou J T, Gershunov A, Guzman-Morales J, Bishop D A, Balch J K and Lettenmaier D P 2019 Observed impacts of anthropogenic climate change on wildfire in California *Earth's Future* 7 892–910
- Williams J W, Jackson S T and Kutzbach J E 2007 Projected distributions of novel and disappearing climates by 2100 AD *Proc. Natl. Acad. Sci. USA* 104 5738–42
- Wu W, Ji F, Hu S and He Y 2024 Asymmetric drying and wetting trends in Eastern and Western China Adv. Atmos. Sci. 41 221–32
- Wu Z and Huang N E 2009 Ensemble empirical mode decomposition: a noise-assisted data analysis method *Adv. Atmos. Sci.* 1 1–41
- Wu Z, Huang N E and Chen X 2009 The multi-dimensional ensemble empirical mode decomposition method Adv. Adapt. Data Anal. 1 339–72
- Wu Z, Huang N E, Long S R and Peng C-K 2007 On the trend, detrending and variability of nonlinear and non-stationary time series *Proc. Natl Acad. Sci. USA* 104 14889–94
- Xu L, Wang A, Wang D and Wang H 2019 Hot spots of climate extremes in the future *J. Geophys. Res.* **124** 3035–49
- Xu L, Wang A, Yu W and Yang S 2021a Hot spots of extreme precipitation change under 1.5 and 2 °C global warming scenarios Weather Clim. Extremes 33 100357
- Xu Z, Ji F, Liu B, Feng T, Gao Y, He Y and Chang F 2021b Long-term evolution of global sea surface temperature trend Int. J. Climatol. 41 4494–508
- Yao T D, Liu X D, Wang N L and Shi Y F 2000 Amplitude of climatic changes in Qinghai-Tibetan Plateau *Chin. Sci. Bull.* **45** 1236–43
- Yin Q, Wang J, Ren Z, Li J and Guo Y 2019 Mapping the increased minimum mortality temperatures in the context of global climate change *Nat. Commun.* **10** 4640
- You Q *et al* 2021 Warming amplification over the Arctic pole and third pole: trends, mechanisms and consequences *Earth Sci. Rev.* 217 103625
- Zhang B, Wang S and Slater L 2024 Anthropogenic climate change doubled the frequency of compound drought and heatwaves in low-income regions *Commun. Earth Environ.* **5** 715
- Zhang J, Wang S, Huang J, He Y and Ren Y 2023 The precipitation-recycling process enhanced extreme precipitation in Xinjiang, China *Geophys. Res. Lett.* **50** e2023GL104324
- Zhao W, Hu Z, Guo Q, Wu G, Chen R and Li S 2020 Contributions of climatic factors to interannual variability of the vegetation index in Northern China grasslands *J. Clim.* 33 175–83
- Zhou T and Zhang W 2021 Anthropogenic warming of Tibetan Plateau and constrained future projection *Environ. Res. Lett.* **16** 044039